Inverse Obstacle Scattering for Homogeneous Dielectric Cylinders Using a Boundary Finite-Element Method

Stéphane Bonnard, Patrick Vincent, and Marc Saillard

***Abstract*—A method for reconstructing the shape and the permittivity of a penetrable homogeneous cylinder is described. It is the extension to penetrable cylinders of a previous work dealing with perfectly conducting cylinders. A low-frequency approximation is used to determine an initial guess. Then, a rigorous boundary integral method permits us to reconstruct arbitrary shapes and complex permittivities. It is based on an iterative conjugate gradient algorithm requiring the solving of two direct diffraction problems only. A simple and original regularization scheme is presented, which ensures the robustness of the algorithm. Numerical examples with lossy embedding media and additional random noise for both $E//$ and $H//$ polarizations are given.**

***Index Terms*—Boundary integral equations, dielectric cylinders, electromagnetic scattering inverse problems, finite-element method.**

I. Introduction

THE use of electromagnetic waves for remote sensing, medical imaging, or subsoil probing applications leads to a wide variety of inverse scattering problems. Generally, depending on the application domain, the pertinent parameters are the location and shape of homogeneous objects or the map of permittivity inside a test area. In this paper, we focus both on the reconstruction of the shape of homogeneous penetrable bodies and on the estimation of their permittivity and conductivity. The geometrical and electromagnetic parameters are found separately through two different optimization subroutines called several times alternatively. The set of data available from measurements also plays an important role. When a horizontal interface takes place between the operator and the target, one must deal with a reduced set of data. Indeed, the antennas are located along a vertical or a horizontal line, depending on whether an invasive or a noninvasive technique is used, respectively. The geometry under study in this paper, referred as a cross-borehole configuration [1]–[3], consists in two parallel wells typically separated by about 100 m. It is devoted to the detection of deep inhomogeneities. The antennas emit a time-harmonic electromagnetic field whose frequency has to satisfy a compromise between penetration and resolution as a result of the strong losses that may occur in the subsoil. Consequently, the size of the inclusions remains smaller than or close to the wavelength in the embedding medium, in general. This explains why in this paper a low-frequency approximation is used for the derivation of an initial guess.

A great variety of methods have been developed to investigate inverse problems. Most of them require a forward solver, even though recent works have shown it is not needed to ensure the efficiency of an algorithm [4]–[6]. In addition, if the nonlinear inverse problem is transformed into an optimization process based on iterative methods, a large number of direct diffraction problems must be solved. Therefore, the speed of reconstruction mainly depends on how fast the forward solver is and on how many such computations are needed at each step. From this numerical point of view, the most efficient methods are those based on Born approximation, but they are restricted to low contrasts of conductivity. A refinement based on a localized nonlinear approximation [7] has been applied to inverse scattering [1], [2] in two and 2.5-dimensional problems, but it also suffers some lack of generality since it requires a highly conducting embedding medium to be accurate. Here, we have already assumed that the various domains are homogeneous. As far as we limit our investigations to cylindrical scatterers, using a rigorous boundary integral formalism able to deal with arbitrary geometries and large contrasts of conductivity represents a reasonable computational effort [8]–[10]. This is no longer true for three-dimensional (3-D) electromagnetic problems. This explains why beyond Born approximation, only few studies exist on this topic [11], [12].

But the key point remains the number of direct problems solved at each step of the iterative scheme. For recent years, theoretical efforts have been achieved in applied mathematics to provide means of determining the Frechet derivative of the cost function from the solution of a few direct problems [13]–[15]. In [15] Hettlich proves that the determination of the functional derivative of the operator mapping the boundary onto the far-field pattern only requires the solving of another boundary value problem. This result applies to acoustic scattering (scalar Helmholtz equation) for any usual boundary conditions, namely the Dirichlet, Neumann, and transmission problems. Therefore, as far as one is concerned with two-dimensional (2-D) electromagnetic inverse problems, algorithms devoted to the reconstruction of a boundary can be built on this basis. Following these mathematical studies, iterative methods have been proposed for numerical applications, using a quasi-Newton minimization for the Dirichlet [16] and Neumann [17] problems, or a Landweber iteration for both the Neumann and the

Manuscript received August 27, 1998; revised August 2, 1999.

The authors are with Laboratoire d'Optique Électromagnétique, CNRS UPRES A 6079, Campus de Saint-Jérôme, F-13397 Marseille Cedex 20, France.

Publisher Item Identifier S 0018-926X(00)02448-0.

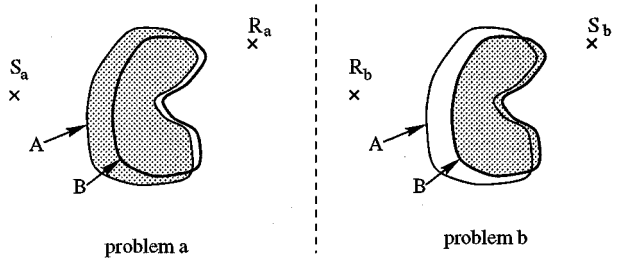

Fig. 1. The two diffraction problems used to compute the gradient formula.

transmission problem [15], [17]. In these latter papers, the inverse problem is formulated in such a way that each iteration step only requires the solving of two identical boundary value problems just with different incident fields. This is exactly the same conclusion Roger [18] has previously derived thanks to the Lorenz reciprocity relation. Indeed, one can express the variations of the field linked to boundary displacements from the solution of two reciprocal direct diffraction problems. As an advantage, this approach is based on Maxwell's equations instead of the scalar Helmholtz equation, thus remains valid for 3-D problems. It has been successfully applied to shape reconstruction of perfectly conducting gratings [19] and cylinders with either complete [20] or reduced set of data [10]. The present paper generalizes [10] to the case of penetrable objects.

II. Theory

The mathematical model used in this paper is 2-D. The embedding medium $\mathcal{D}$ is assumed to be infinite and homogeneous with relative permittivity ϵ_r, conductivity σ, and permeability $\mu = \mu_0$. The scatterers $\mathcal{D}_i$ are homogeneous cylinders with relative permittivity $\epsilon_{r,i}$, conductivity σ_i, and permeability $\mu_i = \mu_0$. The cross sections are arbitrary. For the sake of simplicity, the equations are established with one cylinder and the boundary of $\mathcal{D}_i$ is denoted by A but the generalization to several cylinders is straightforward.

A right-handed Cartesian coordinate frame $(O, \boldsymbol{e_x}, \boldsymbol{e_y}, \boldsymbol{e_z})$ is defined. The origin O could be either inside or outside the scatterer and the y-axis is parallel to the axis of the scatterer. When needed, cylindrical coordinates (r, θ, y) are also used and the position vector OM is written

$$OM = x\,\boldsymbol{e_x} + y\,\boldsymbol{e_y} + z\,\boldsymbol{e_z} = \boldsymbol{r} + y\,\boldsymbol{e_y}. \tag{1}$$

The unit normal vector $\boldsymbol{n}$ to the scatterer is directed outwards the cylinder and the unit tangential vector is defined by: $\boldsymbol{t} = \boldsymbol{n} \times \boldsymbol{e_y}$.

The sources are assumed to be lines parallel to the y-axis, thus, the diffraction problem can be reduced to a 2-D one with two fundamental cases of polarization: the $E//$ case when the electric field is parallel to the y-axis and the $H//$ case when the magnetic field is parallel to the y-axis. Taking into account a time dependence in $\exp(j\omega t)$, in the $E//$ case, the time-harmonic incident electric field is written

$$\boldsymbol{U^i}(\boldsymbol{r}) = \boldsymbol{E^i}(\boldsymbol{r}) = U^i(\boldsymbol{r})\boldsymbol{e_y} = -\boldsymbol{P}\frac{\omega\mu}{4}H_0^{(2)}(kr) \tag{2}$$

where

- $\boldsymbol{P}$ strength of the electric source;
- ω angular frequency;
- $H_0^{(2)}$ Hankel function of zero order and second kind;
- k wavenumber in the surrounding medium;
- r $= |\boldsymbol{r}|$.

In the $H//$ case of polarization, the magnetic field component used is

$$\boldsymbol{U^i}(\boldsymbol{r}) = \boldsymbol{H^i}(\boldsymbol{r}) = U^i(\boldsymbol{r})\boldsymbol{e_y} = \boldsymbol{M}\frac{\omega\epsilon}{4}H_0^{(2)}(kr) \tag{3}$$

where $\boldsymbol{M}$ is the strength of the magnetic source and ϵ_0 is the free-space permittivity. In a typical configuration, the sources and the receivers are located in two parallel boreholes.

Taking into account the time-dependence factor, the complex permittivity of each medium is given by

$$\epsilon = \epsilon_0\epsilon_r - \frac{j\sigma}{\omega} \tag{4}$$

$$\epsilon_i = \epsilon_0\epsilon_{r,i} - \frac{j\sigma_i}{\omega}. \tag{5}$$

A. Integral Equation

The forward 2-D problem is solved thanks to a boundary integral equation using the Kirchhoff–Helmholtz formula.

Let us define a function $F(x, z)$, which satisfies a radiation condition at infinity and

- $F = U^d$ the diffracted field in $\mathcal{D}$;
- $\Delta F + k^2 F = 0$ in $\mathcal{D} \cup \mathcal{D}_i$ (i.e., everywhere except on $\boldsymbol{A}$);
- F is continuous across A.

Let ϕ be the jump of the normal derivative of $\boldsymbol{F}$ across the boundary A: this unknown function satisfies the boundary integral equation written in the operator form [21], [22]

$$\left[\left(\frac{1}{2} - \frac{d\boldsymbol{G}_i}{dn'}\right)\boldsymbol{G} + \alpha_i\boldsymbol{G}_i\left(\frac{1}{2} + \frac{d\boldsymbol{G}}{dn}\right)\right]\phi = -\left(\frac{1}{2} - \frac{d\boldsymbol{G}_i}{dn'}\right)U^i - \alpha_i\boldsymbol{G}_i\frac{dU^i}{dn} \tag{6}$$

where

- $\boldsymbol{G}$ is the 2-D free-space Green integral operator defined by

$$\boldsymbol{G}\phi = \int_A G(\boldsymbol{r}, \boldsymbol{r}')\phi(\boldsymbol{r}')\,ds'$$

with

$$G(\boldsymbol{r}, \boldsymbol{r}') = \frac{j}{4}H_0^{(2)}(k|\boldsymbol{r} - \boldsymbol{r}'|)$$

- $\boldsymbol{G}_i$ is defined similarly but with the wavenumber k_i inside the scatterer;
- $d\boldsymbol{G}/dn$ is the normal derivative computed at $\boldsymbol{r}$;
- $d\boldsymbol{G}_i/dn'$ is the normal derivative computed at $\boldsymbol{r'}$;
-

$$\alpha_i = \begin{cases} \dfrac{\mu_i}{\mu} & \text{in the } E// \text{ case of polarization,} \\ \dfrac{\epsilon_i}{\epsilon} & \text{in the } H// \text{ case of polarization.} \end{cases}$$

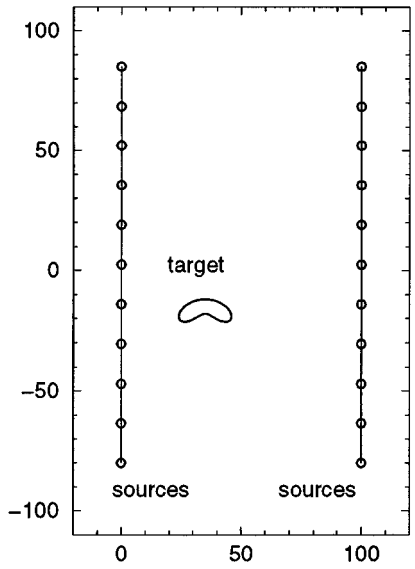

Fig. 2. Layout of the boreholes and the target.

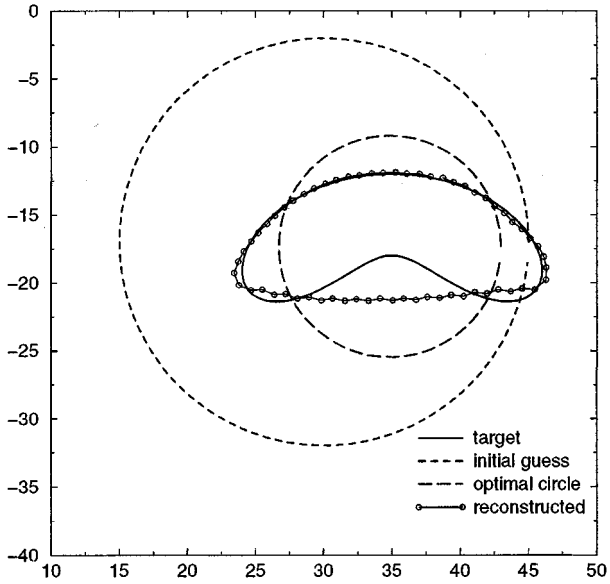

Fig. 3. Example of reconstruction in s polarization ($E//$) without noise in the measured field.

Then, the knowledge of the function ϕ on the boundary allows us to calculate the scattered field at any point of the embedding medium by the formula

$$U^d(\boldsymbol{r}) = \boldsymbol{G}\phi = \int_A G(\boldsymbol{r}, \boldsymbol{r}')\phi(\boldsymbol{r}')\, ds'. \tag{7}$$

B. Boundary Finite-Element Method

The integral equation is transformed into a linear system using a Galerkin scheme. First, the boundary is approximated by a polygonal line composed of N straight segments whose vertices are on the true boundary. Then, the unknown function ϕ is written as a sum of piecewise constant basis functions φ_n, normed with respect to the scalar product

$$(\varphi_n, \varphi_m) = \int_{\boldsymbol{A}} \varphi_n(s)\varphi_m(s)\, ds. \tag{8}$$

Each function φ_n is nonnull on a side of the polygon and zero elsewhere and the equations are projected onto the same test functions. The result is a dense linear system of N equations solved by a classical LU decomposition. For typical examples, N varies from 50 to 100.

C. Cost Functional

The aim of the computation is to determine the shape and the constitutive parameters of the diffracting cylinder assuming that the permittivity of the embedding medium, the incident field and the values of the diffracted field measured in the receiving boreholes are known. The shape and the permittivity are alternatively determined in an iterative manner in order to minimize a cost functional, which gives the normalized deviation between the computed field and the measured field. In both cases of polarization, this cost functional is defined by

$$F(\boldsymbol{A}, \epsilon_{\boldsymbol{i}}) = \sum_{m=1}^{N_m} \frac{|U_m^{\text{calc}}(\boldsymbol{A}, \epsilon_{\boldsymbol{i}}) - U_m^{\text{mes}}|^2}{|U_m^{\text{mes}}|^2} \tag{9}$$

where

- N_m number of measurements in different points along the boreholes;
- U_m^{mes} mth measured field value;
- U_m^{calc} mth calculated field from the estimated profile $\boldsymbol{A}$ or from the estimated complex permittivity ϵ_i.

D. Shape Reconstruction

The minimization of the above cost functional is performed by a conjugate gradient method with linear search of the minimum in the conjugate direction. In order to find a new shape at each step of the iterative algorithm, the functional derivative of F is needed. If δU_m^{calc} is a given change in the computed field, a simple differentiation yields

$$\delta F = 2 \sum_{m=1}^{N_m} \Re e \left[\overline{\left(\frac{U_m^{\text{calc}} - U_m^{\text{mes}}}{U_m^{\text{mes}}} \right)} \frac{\delta U_m^{\text{calc}}}{U_m^{\text{mes}}} \right] \tag{10}$$

where the overbar denotes complex conjugate.

The adjoint state method [18], already used by the authors of this paper for infinitely conducting cylinders [10], is used here to calculate δU_m^{calc} as a function of the shape $\boldsymbol{A}$. For that, two diffraction problems a and b depicted in Fig. 1 are defined. For problem a with an electric source at point S_a Maxwell's equations yield

$$\nabla \times \boldsymbol{E}_a = -j\omega\mu_0 \boldsymbol{H}_a \tag{11}$$

$$\nabla \times \boldsymbol{H}_a = j\omega\epsilon_a \boldsymbol{E}_a + \boldsymbol{P}_a \delta(\boldsymbol{r} - \boldsymbol{S}_a) \tag{12}$$

where δ is the Dirac distribution and ϵ_a equals ϵ_i inside the cylinder and ϵ outside. For a magnetic source, these equations are changed into

$$\nabla \times \boldsymbol{E}_a = -j\omega\mu_0 \boldsymbol{H}_a + \boldsymbol{M}_a \delta(\boldsymbol{r} - \boldsymbol{S}_a) \tag{13}$$

$$\nabla \times \boldsymbol{H}_a = j\omega\epsilon_a \boldsymbol{E}_a. \tag{14}$$

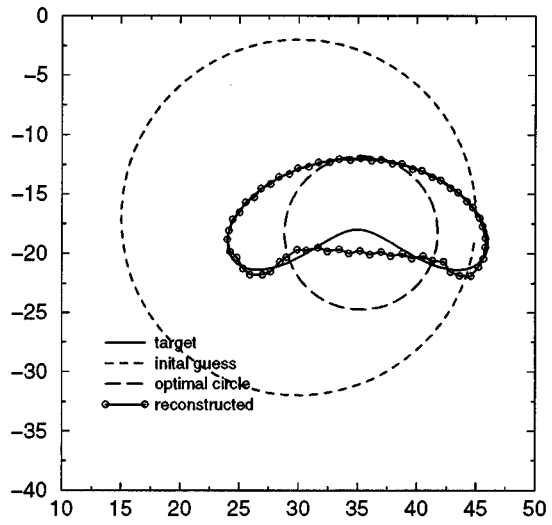

Fig. 4. Example of reconstruction in p polarization ($H//$) without noise in the measured field.

The diffraction problem b is defined with the same polarization and the same permittivities ϵ and ϵ_i, but with a different cylinder shape $\boldsymbol{B}$ and a different source location S_b. Assuming that there is no incoming wave at infinity, the Lorentz reciprocity relation can be written as

$$\iint_{\text{all space}} \nabla \cdot (\boldsymbol{H}_b \times \boldsymbol{E}_a - \boldsymbol{H}_a \times \boldsymbol{E}_b)\, d\Omega = 0. \tag{15}$$

Taking into account Maxwell's equations and changing the divergence integral into a boundary integral, for the $E//$ case of polarization, a classical computation yields

$$\begin{aligned}\boldsymbol{E}_b(\boldsymbol{S}_a) \cdot \boldsymbol{P}_a - \boldsymbol{E}_a(\boldsymbol{S}_b) \cdot \boldsymbol{P}_b \\ = j\omega \iint_\Omega (\epsilon_b - \epsilon_a) E_a\, E_b\, d\Omega.\end{aligned} \tag{16}$$

Note that the integration domain for the right-hand member is the region Ω where $\epsilon_b \neq \epsilon_a$. In the following, it is assumed that $\boldsymbol{r}_1 = \boldsymbol{S}_a = \boldsymbol{R}_b$, $\boldsymbol{r}_2 = \boldsymbol{S}_b = \boldsymbol{R}_a$, and $\boldsymbol{P} = \boldsymbol{P}_a = \boldsymbol{P}_b$, thus

$$\boldsymbol{E}_b(\boldsymbol{S}_a) \cdot \boldsymbol{P}_a - \boldsymbol{E}_a(\boldsymbol{S}_b) \cdot \boldsymbol{P}_b = [\boldsymbol{E}_b(\boldsymbol{r}_1) - \boldsymbol{E}_a(\boldsymbol{r}_2)] \cdot \boldsymbol{P}. \tag{17}$$

Let us define a new diffraction problem b' by exchanging the source and the receiver in b. Hence, the classical reciprocity theorem applies

$$\boldsymbol{E}_b(\boldsymbol{r}_1) \cdot \boldsymbol{P} = \boldsymbol{E}_{b'}(\boldsymbol{r}_2) \cdot \boldsymbol{P}. \tag{18}$$

Noting that problems a and b' differ only by the cylinder shape and introducing $\delta \boldsymbol{E}_a = \boldsymbol{E}_{b'} - \boldsymbol{E}_a$, (16) can be rewritten as

$$\delta \boldsymbol{E}_a(\boldsymbol{r}_2) \cdot \boldsymbol{P} = j\omega \iint_\Omega (\epsilon_b - \epsilon_a) E_a\, E_b\, d\Omega. \tag{19}$$

Now let us introduce $\boldsymbol{E}_{a'}$, the field in the diffraction problem a' defined by exchanging the source and the receiver in problem a. Assuming that the shape $\boldsymbol{B}$ is close to $\boldsymbol{A}$, we note δA the shift measured along the normal $\boldsymbol{n}$. It comes out that

$$E_a\, E_b = E_a\, E_{a'} + o(\delta A). \tag{20}$$

Noting that $d\Omega = |\delta A\, ds|$ and

$$\begin{aligned}&\text{if } \delta A > 0: \quad \epsilon_b - \epsilon_a = \epsilon_i - \epsilon \\ &\text{if } \delta A < 0: \quad \epsilon_b - \epsilon_a = \epsilon - \epsilon_i\end{aligned}$$

it is possible to write, up to first order in δA, the functional derivative as a simple boundary integral of the solution of two forward diffraction problems

$$\delta \boldsymbol{E}_a(\boldsymbol{r}_2) \cdot \boldsymbol{P} \simeq j\omega(\epsilon_i - \epsilon) \int_{\boldsymbol{A}} E_a\, E_{a'}\, \delta A\, ds. \tag{21}$$

The value of the electric field on the boundary is obtained from the solution ϕ of the integral equation by the following formula [22]:

$$E = e_i + \boldsymbol{G}\phi \tag{22}$$

where e_i is the value of the electric incident field on $\boldsymbol{A}$.

In the $H//$ case of polarization (16) is changed into

$$\begin{aligned}\boldsymbol{H}_b(\boldsymbol{S}_a) \cdot \boldsymbol{M}_a - \boldsymbol{H}_a(\boldsymbol{S}_b) \cdot \boldsymbol{M}_b \\ = j\omega \iint_\Omega (\epsilon_a - \epsilon_b) \boldsymbol{E}_a \cdot \boldsymbol{E}_b\, d\Omega.\end{aligned} \tag{23}$$

and (19) replaced by

$$\delta \boldsymbol{H}_a(\boldsymbol{r}_2) \cdot \boldsymbol{M} = j\omega \iint_\Omega (\epsilon_a - \epsilon_b) \boldsymbol{E}_a \cdot \boldsymbol{E}_b\, d\Omega. \tag{24}$$

In this case, the electric field is perpendicular to the cylinder axis. Hence, it can be written $\boldsymbol{E} = E^t \boldsymbol{t} + E^n \boldsymbol{n}$ and we get

$$\begin{aligned}\boldsymbol{E}_a \cdot \boldsymbol{E}_b &\simeq E_a^t \cdot E_{a'}^t + E_a^n \cdot E_{a'}^n \\ &\simeq -\frac{1}{\omega^2 \epsilon_i \epsilon} \left(\frac{\epsilon_i}{\epsilon} \frac{dH_a}{dn}^+ \frac{dH_{a'}}{dn}^+ + \frac{dH_a}{dt} \frac{dH_{a'}}{dt} \right)\end{aligned} \tag{25}$$

where the superscript $^+$ denotes that the limit of the function is calculated in the exterior domain and d/dt is the tangential derivative. As a result, (21) is changed in a more complicated relation

$$\begin{aligned}\delta \boldsymbol{H}_a(\boldsymbol{r}_2) \cdot \boldsymbol{M} = \frac{1}{j\omega} \int_{\boldsymbol{A}} \left[\frac{1}{\epsilon} \left(\frac{\epsilon_i}{\epsilon} - 1 \right) \frac{dH_a}{dn}^+ \frac{dH_{a'}}{dn}^+ \right. \\ \left. + \frac{1}{\epsilon_i} \left(\frac{\epsilon_i}{\epsilon} - 1 \right) \frac{dH_a}{dt} \frac{dH_{a'}}{dt} \right] \delta A\, ds.\end{aligned} \tag{26}$$

In this case of polarization, the normal and tangential derivative are computed from the solution ϕ by [22]

$$\frac{dH}{dn}^+ = \frac{dh_i}{dn} + \left(\frac{1}{2} + \frac{d\boldsymbol{G}}{dn} \right) \phi \tag{27}$$

$$\frac{dH}{dt} = \frac{dh_i}{dt} + \frac{d\boldsymbol{G}}{dt} \phi. \tag{28}$$

E. Constitutive Parameters

The determination of the complex permittivity is also achieved by minimizing the cost functional described in Section II-C. This time, the profile $\boldsymbol{A}$ of the cylinder is fixed and a different iterative gradient method is used because the computation of the components of the gradient with respect to

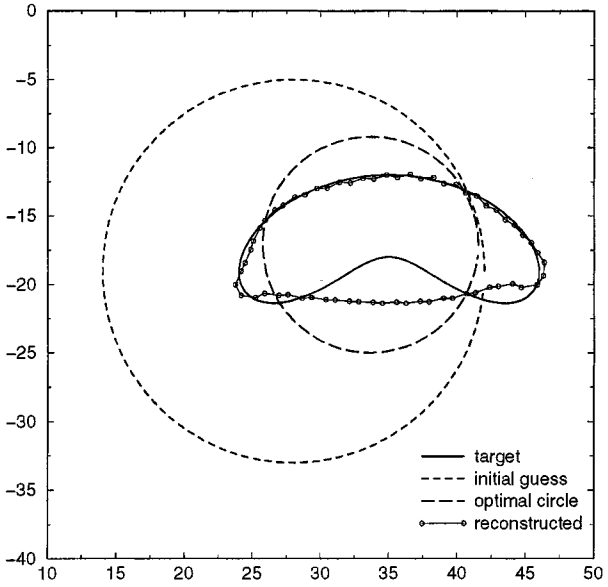

Fig. 5. Same as in Fig. 3, but with 30% noise added.

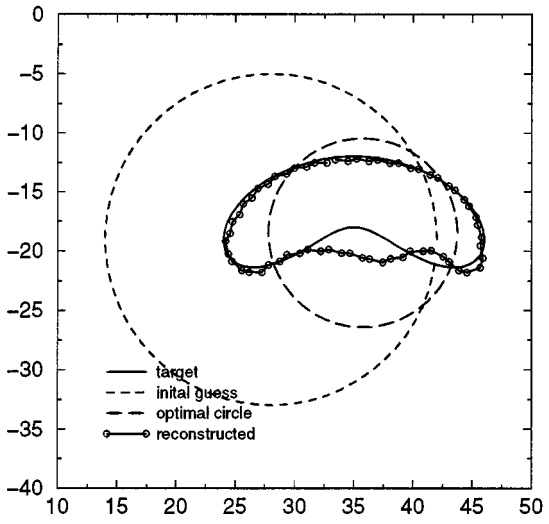

Fig. 6. Same as in Fig. 4, but with 30% noise added.

the permittivity ϵ_i gives a complicated result. More precisely, it is easily shown that

$$\frac{\delta U^{\text{calc}}}{\delta \epsilon_i}(\boldsymbol{r}) = \int_A G(\boldsymbol{r}, \boldsymbol{r}') \frac{\delta \phi}{\delta \epsilon_i}(\boldsymbol{r}')\, ds' = \boldsymbol{G} \frac{\delta \phi}{\delta \epsilon_i} \tag{29}$$

but the computation of $(\delta\phi)/(\delta\epsilon_i)$ yields a rather complicated formula. Hence, taking into account the small number of unknown parameters (two real parameters per cylinder: $\epsilon_{r,i}$ and σ_i) a numerical determination of the gradient is a logical choice. We choose a standard optimization program called PRAXIS based on Brent's method [23], i.e., an inverse parabolic interpolation. To avoid negative values for ϵ_i and σ_i it has been necessary to impose the positivity of the unknown parameters. This is done by a change of variables: the new unknowns (X_i, Y_i) are defined by

$$\epsilon_{r,i} = 1 + X_i^2 \tag{30}$$

$$\sigma_i = Y_i^2. \tag{31}$$

This choice has proven to be very efficient chiefly concerning $\epsilon_{r,i}$. The PRAXIS procedure also uses two auxiliary input parameters called $T0$ and $H0$ requiring an adequate choice. $T0$ is a tolerance such as $|X - X0| \leq T0$, where $X0$ is the true local minimum and X the value that PRAXIS attempts to return. $H0$ is the maximum step size which should be about the maximum distance from the initial guess to the minimum. Numerical experiments have shown that for the typical examples described in the following section, the optimum values are about 10^{-1} for $T0$ and 10 for $H0$. It is worth noticing that these two parameters do not change the values of the results but have a strong effect on the velocity of convergence of the program, which reaches a stable value after about 1 min on a 25 Mflops desktop workstation.

In fact, a two-level iteration is performed; having determined the constitutive parameters corresponding to a given shape, a new cycle is started beginning with a new shape reconstruction iteration until the global stabilization is achieved.

F. Initial Guess

A low-frequency approximation method to find an initial guess for the location, size, and permittivity of the cylinder is described in this section. This method is based on the isotropy of the scattered field for low frequencies in the $E//$ case of polarization when only one object is located between the two boreholes. This isotropy occurs independently of the shape of the scatterer. Therefore, we look for a circular shape with center C, radius r_0 and complex permittivity $\tilde{\epsilon}_i$.

Assuming that the incident field is a cylindrical wave centered at the point $S = (r_S, \theta_S)$, according to Graf's formula [24], the scattered field outside the object in the direction θ can be expanded as

$$E^d(r, \theta) = \sum_{n=-\infty}^{\infty} b_n H_n^{(2)}(k|\boldsymbol{r}_S - \boldsymbol{r}_C|) \cdot H_n^{(2)}(k|\boldsymbol{r} - \boldsymbol{r}_C|)\, e^{jn(\theta - \theta_S)}. \tag{32}$$

When the profile is circular, the coefficients b_n can be written in close form using the continuity conditions at $r = r_0$. In our case, the term b_0 is dominating and we have

$$E^d(r, \theta) \simeq b_0 H_0^{(2)}(k|\boldsymbol{r}_S - \boldsymbol{r}_C|) H_0^{(2)}(k|\boldsymbol{r} - \boldsymbol{r}_C|). \tag{33}$$

For a given abscissa x_R of the receivers, the maximum of the modulus of the measured scattered field coincides with the depth of the object. This depth gives the ordinate of the center of the circle.

The computation of the abscissa x_C of the center of the circle is performed with the values of the diffracted field measured in two different points $R_1 = (x_R, z_1)$ and $R_2 = (x_R, z_2)$, with

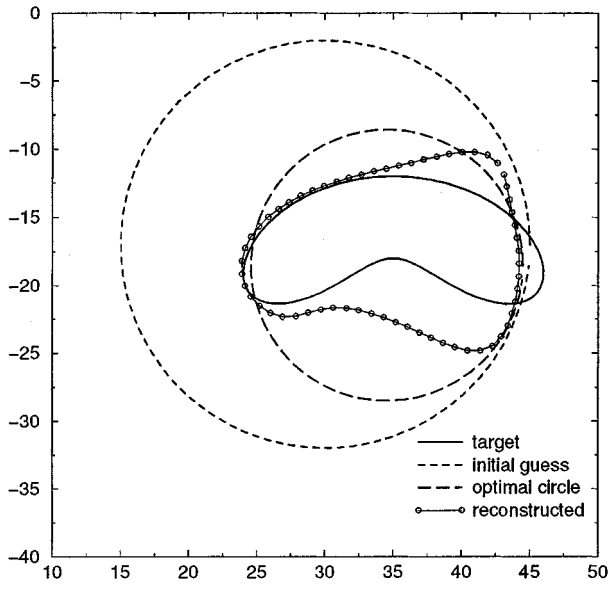

Fig. 7. Reconstruction without noise, in s polarization ($E//$), in a single-well configuration.

$E^{\mathrm{mes}}(x_R, z_1) \neq E^{\mathrm{mes}}(x_R, z_2)$. Using the asymptotic expansion of Hankel's functions, this leads to an implicit equation in x_C

$$\ln\left|\frac{E^{\mathrm{mes}}(x_R, z_1)}{E^{\mathrm{mes}}(x_R, z_2)}\right| = \frac{1}{2}\ln\left(\frac{r_2}{r_1}\right) + \Im m[k(r_2 - r_1)] \quad (34)$$

where for $i = 1, 2$, $r_i = \sqrt{(x_C - x_R)^2 + (z_C - z_i)^2}$.

The determination of the radius r_0 and the complex permittivity $\tilde{\epsilon}_i$ requires two steps because it can be shown that for small arguments

$$b_0 \sim j\frac{\pi}{4}(kr_0)^2\left(1 - \frac{\tilde{\epsilon}_i}{\epsilon}\right) \quad (35)$$

thus, the diffracted field only depends on the parameter

$$P = r_0^2\left(1 - \frac{\tilde{\epsilon}_i}{\epsilon}\right). \quad (36)$$

The optimal value of $P = P_{\min}$ found by minimizing the cost function

$$F_C(P) = \sum_{m=1}^{N_m}\left|E_m^d(P) - E_m^{\mathrm{mes}}\right|^2 \quad (37)$$

is

$$P_{\min} = \frac{4}{j\pi k^2}\frac{\sum_{m=1}^{N_m}\overline{H_0^{(2)}(kr_m)}\,E_m^{\mathrm{mes}}}{\sum_{m=1}^{N_m}\left|H_0^{(2)}(kr_m)\right|^2}. \quad (38)$$

It is possible to write explicitly the relative permittivity $\tilde{\epsilon}_{r,i}$ and the conductivity $\tilde{\sigma}_i$ as functions of $P_{\min}$, but, in fact, the formula giving $\tilde{\epsilon}_{r,i}$ leads to bad results if the radius of the circle is not the true one and a good choice is simply to take $\tilde{\epsilon}_{r,i} = 1$. Noticing that in the low-frequency range the imaginary part of P can be neglected, the initial guess for the conductivity is finally

$$\tilde{\sigma}_i = \sigma\left(1 - \frac{\Re e(P_{\min})}{r_0^2}\right). \quad (39)$$

The last parameter needed to start the iteration is the radius r_0 of the circle. Two cases must be distinguished according to the sign of $\Re e(P_{\min})$

- if $\Re e(P_{\min}) > 0$, the conductivity of the scatterer σ_i is smaller than the conductivity σ of the embedding medium and $\Re e(P_{\min})) \simeq r_0^2$ gives a good choice for r_0;
- if $\Re e(P_{\min}) < 0$, the preceding criterion does not apply and we start from a radius equal to half the distance from the center of our initial guess to the nearest borehole.

G. Regularization

In the shape reconstruction process, the profile is first approximated by a polygonal closed line of N segments with vertices on the true profile, then the cost functional F is minimized by computing the displacement $\delta\boldsymbol{M_n}$ of the middle of each segment along the normal. At each step of the iteration, new vertices $\boldsymbol{v}_i$ must be determined from the position of the middle $\boldsymbol{m}_i$ of the ith side of the polygon. It is easy to see that the solution of this problem is undetermined if the number N of vertices is even, thus, we take an odd value for N. In that case, a straightforward calculation gives

$$\boldsymbol{v}_1 = \sum_{i=1}^{N}(-1)^{i-1}\boldsymbol{m}_i \quad \text{and} \quad \boldsymbol{v}_{i+1} = 2\boldsymbol{m}_i - \boldsymbol{v}_i. \quad (40)$$

In fact, we noted that the instability of the inverse method concentrates essentially in the above formula and that after few iterations the middle points remain regularly located, but the polygonal shape become very irregular. The method used to avoid these instabilities is very simple and purely geometrical [10]. It is logical to think that if the diffracting object is well represented by a polygon, the slight change made by taking the middle points as vertices, i.e., to write

$$\boldsymbol{v}_i = \boldsymbol{m}_i \quad (41)$$

must not change significantly the diffraction pattern. Hence, at each step of the iteration we compare the perimeter of two polygons with vertices from (40) or (41). If the difference is less than 5% (40) is used; if not, (41) is used and the conjugate gradient is reinitialized. This geometrical regularization has proven to be efficient and, as simulated annealing methods do, gives an opportunity to get out of local minima. Contrary to a Tikhonov regularization, it is not worth looking for a judicious value of the parameter which balances the error term and the regularization one in the cost functional.

III. Numerical Results

To point out the versatility of the method, we vary the polarization and the number of boreholes for a given non convex object. The background conductivity is set to $\sigma = 10^{-3}$ Sm^{-1}, while the real part of the permittivity is equal to one. First, we consider two boreholes 100 m far from each other. Along each

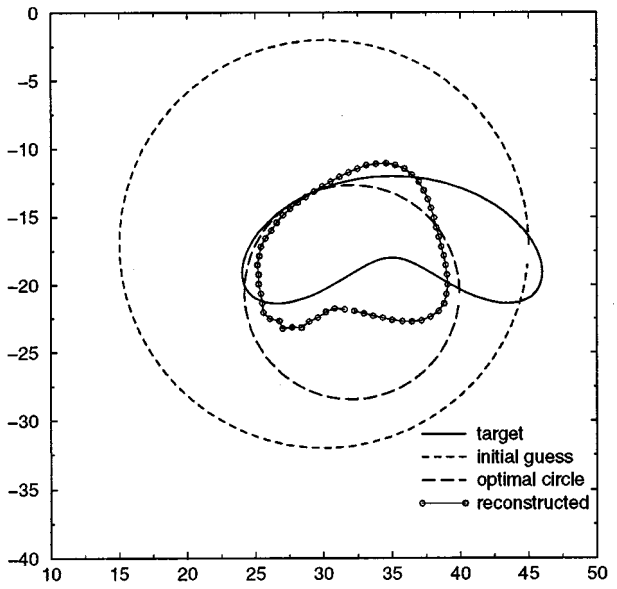

Fig. 8. Reconstruction without noise in p polarization ($H//$) in a single-well configuration.

borehole, 11 locations of the emitters and receivers are regularly spaced between $z = -80$ m and $z = 85$ m. The operating frequency is 5 MHz corresponding to a wavelength in the embedding medium about 40 m, i.e., approximately twice the distance between two consecutive points of measurement.

The size of the object is approximately 22 m $\times$ 10 m and its shape is looking like a bean (Fig. 2); it is given by

$$x = \quad 35 + 10\cos\theta - 2.5\sin 2\theta \tag{42}$$

$$z = -18 + 3\sin\theta - 3\cos 2\theta. \tag{43}$$

The constitutive parameters of this dielectric "bean" are $\epsilon_{r,i} = 1$ and $\sigma_i = 0.1$ Sm^{-1}. The initial guess is found with a lower frequency of 10 kHz. It is represented in Figs. 3 and 4 by the dashed curve.

Using simulated data at 5 MHz without noise, we have found, in both cases of polarization, an optimal circle well centered on the target represented by the long-dashed curve (Figs. 3 and 4). For each optimal circle, we found $\tilde{\epsilon}_{r,i} = 1$, $\tilde{\sigma}_i = 0.16$ S/m in s polarization, and $\tilde{\epsilon}_{r,i} = 1$ and $\tilde{\sigma}_i = 0.022$ S/m in p polarization. Going on with an arbitrary boundary, we are lead to the curve marked with white circles, close to the true one and the new estimated electromagnetic parameters $\epsilon_{r,i} = 1$, $\sigma_i = 0.104$ S/m in s polarization and $\epsilon_{r,i} = 1$, $\sigma_i = 0.085$ S/m in p polarization.

The same experiments are repeated by introducing some noise in the data. The field E_m^{calc} calculated by solving the forward diffraction problem is perturbed according to

$$E_m^{\text{mes}} = E_m^{\text{calc}}\left(1 + be^{i\phi_m}\right) \tag{44}$$

where $b = 0.3$ and $\{\phi_m\}$ is a random set equally distributed in $[0, 2\pi]$. Results in Figs. 5 and 6 show a good robutness of the method against noise.

Now, let us consider a single-well configuration. We have chosen to keep the left borehole ($x = 0$ m). From simulated data without noise, the reconstruction in both cases of polarization are depicted in Figs. 7 and 8.

We notice a better reconstruction in s polarization than p polarization and also a better reconstruction of the illuminated part of the object. In both cases, the lack of information due to the absence of the second borehole leads to a less accurate reconstruction of the boundary. In the same way, the conductivity is found to be $\sigma_i = 0.022$ S/m in s polarization and $\sigma_i = 0.015$ S/m in p polarization.

IV. Conclusion

The method presented in this paper has permitted us to reconstruct both the boundary and the complex permittivity of a homogeneous cylindrical object with reduced set of data. Thanks to rapid computation of the functional derivative of the cost function, the whole process typically requires a few minutes on a desktop workstation. However, in the present state, several shortcomings still exist. First, the regularization process, though efficient, is not fully satisfactory because it leads to frequent reinitialization of the conjugate gradient algorithm. To overcome this drawback, we plan to implement an other representation of the boundary based on a Fourier representation, in order to ensure its smoothness. Second, boundary integral methods may encounter some difficulties in reconstructing several disconnected objects if the number of scatterers is not known *a priori*. With this aim, a treatment of the data called decomposition of the time reversal operator [25], [26] is studied. The eigenvalues and eigenvectors of this operator contain a lot of information about the number of scatterers and their location. Other methods to seek for the support of disconnected penetrable as well as impenetrable objects can also be considered [27], [28].

Nevertheless, the robustness and the efficiency of the algorithm have been successfully tested against experimental data in an other geometrical configuration. The measurements achieved in our anechoic chamber concern a metallic cylinder placed in air, illuminated by a horn antenna. Future experimental work will deal with one or several penetrable objects.

References

[1] C. Torres-Verdin and T. Habashy, "Rapid 2.5-dimensional forward modeling and inversion via a new nonlinear scattering approximation," *Radio Sci.*, vol. 29, no. 4, pp. 1051–1079, 1994.

[2] ——, "A two-step linear inversion of two-dimensional electrical conductivity," *IEEE Trans. Antennas Propagat.*, vol. 43, pp. 405–415, Apr. 1995.

[3] G. Newman, "Crosswell electromagnetic inversion using integral and differential equations," *Geophys.*, vol. 60, no. 3, pp. 899–911, 1995.

[4] R. E. Kleinman and P. M. van den Berg, "A modified gradient method for two-dimensional problems in tomography," *J. Computat. Appl. Math.*, vol. 42, pp. 17–35, 1992.

[5] ——, "Two-dimensional location and shape reconstruction," *Radio Sci.*, vol. 29, no. 4, pp. 1157–1169, 1994.

[6] K. Belkebir, C. Pichot, and R. E. Kleinman, "Microwave imaging—Location and shape reconstruction from multifrequency scattering data," *IEEE Trans. Microwave Theory Tech.*, vol. 45, pp. 469–476, Apr. 1997.

[7] T. Habashy, R. W. Groom, and B. R. Spies, "Beyond the Born and Rytov approximations: A nonlinear approach to electromagnetic scattering," *J. Geophys. Res.*, vol. 98, pp. 1759–1775, 1993.

[8] C.-C. Chiu and Y.-W. Kiang, "Electromagnetic imaging for an imperfectly conducting cylinder," *IEEE Trans. Microwave Theory Tech.*, vol. 39, no. 9, pp. 1632–39, 1991.

[9] E. Ngakosso, M. Saillard, and P. Vincent, "Electromagnetic diffraction by homogeneous cylinders of the field radiated by a dipole: A rigorous computation," *J. Electromagn. Waves Applicat.*, vol. 9, no. 9, pp. 1189–1205, 1995.

[10] S. Bonnard, P. Vincent, and M. Saillard, "Cross-borehole inverse scattering using a boundary finite element method," *Inverse Problems*, vol. 14, no. 3, pp. 521–534, June 1998.
[11] P. Maponi, M. Recchioni, and F. Zirilli, "Three-dimensional time harmonic electromagnetic inverse scattering-the reconstruction of the shape and the impedance of an obstacle," *Computat. Math. Applicat.*, vol. 31, pp. 1–7, 1996.
[12] J.-H. Lin and W. C. Chew, "Solution of the three-dimensional electromagnetic inverse problem by the local shape function and the conjugate gradient fast Fourier transform methods," *J. Opt. Soc. Amer. A*, vol. 14, no. 11, pp. 3037–3045, 1997.
[13] A. Kirsch, "The domain derivative and two applications in inverse scattering theory," *Inverse Problems*, vol. 9, pp. 81–96, 1993.
[14] R. Potthast, "Frechet differentiability of boundary integral operators," *Inverse Problems*, vol. 10, pp. 431–447, 1994.
[15] F. Hettlich, "Frechet derivatives in inverse obstacle scattering," *Inverse Problems*, vol. 11, pp. 371–382, 1995.
[16] R. Kress and W. Rundell, "A quasi-Newton method in inverse obstacle scattering," *Inverse Problems*, vol. 10, pp. 1145–1157, 1994.
[17] F. Hettlich and W. Rundell, "A quasi-Newton method in inverse obstacle scattering," *Inverse Problems*, vol. 12, pp. 251–266, 1996.
[18] A. Roger, "Reciprocity theorem applied to the computation of functional derivatives of the scattering matrix," *Electromagn.*, vol. 2, pp. 69–83, 1982.
[19] ——, "Optimization of perfectly conducting gratings. A general method," *Optica Acta*, vol. 30, no. 3, pp. 387–398, 1983.
[20] ——, "Problèmes inverses en électromagnétisme. Etude théorique, numérique et résultats expérimentaux," *Revue du Cethedec, Ondes et Signal*, vol. 76, pp. 35–43, 1983.
[21] D. Maystre and P. Vincent, "Diffraction d'une onde électromagnétique plane par un objet cylindrique non infiniment conducteur de section arbitraire," *Opt. Communicat.*, vol. 5, pp. 327–330, 1972.
[22] M. Saillard, P. Vincent, and D. Maystre, "A finite element method for electromagnetic subsurface tomography," *Finite Element Software for Microwave Engineering*, ser. Microwave and Optical Engineering, pp. 237–265, 1996.
[23] W. H. Press, B. P. Flannery, S. A. Teukolsky, and W. T. Vetterling, *Numerical Recipes in FORTRAN*, 1992.
[24] M. Abramowitz and I. A. Stegun, *Handbook of Mathematical Functions*, 10th ed. New York: Dover, 1972.
[25] M. Fink, "Time-reversed acoustics," *Phys. Today*, pp. 34–40, Mar. 1997.
[26] H. Tortel, G. Micolau, and M. Saillard, "Decomposition of the time reversal operator for electromagnetic scattering," *J. Electromagn. Waves Applicat.*, vol. 13, pp. 687–711, 1999.
[27] D. Colton, M. Piana, and R. Potthast, "A simple method using Morozov's discrepancy principle for solving inverse scattering problems," *Inverse Problems*, vol. 13, no. 6, pp. 1477–93, 1997.
[28] A. Litman, D. Lesselier, and F. Santosa, "Reconstruction of a two-dimensional binary obstacle by controlled evolution of a level-set," *Inverse Problems*, vol. 14, pp. 685–706, 1998.

Stéphane Bonnard was born in Aubenas on March 30, 1972. He received the Engineering degree from the Ecole Nationale Supérieure de Physique, Marseille, France, in 1995, and the Ph.D. degree from the University of Aix-Marseille, France, in 1999.

His area of research is electromagnetic inverse problems.

Patrick Vincent was born in Roanne, France, in 1945. He received the Ph.D. degree (Doctorat d'Etates Sciences Physiques) from the Université de Provence, France, in 1978.

He joined the Laboratoire d'Optique Electromagnétique (LOE), Marseille, France, in 1970. He is currently a Professor at the Université d'Aix-Marseille. He is the author of the chapter "Differential Methods" in *Electromagnetic Theory of Gratings* (New York: Springer-Verlag, 1980, R. Petit, Ed.), is coauthor of a chapter in *Finite Element Software for Microwave Engineering* (New York: Wiley, 1996), and is also coauthor of about 50 papers in the field of electromagnetic diffraction. He is interested in the numerical computation of the direct and inverse diffraction of electromagnetic waves by objects in the resonance region. His research interests include inverse scattering and photonic crystals.

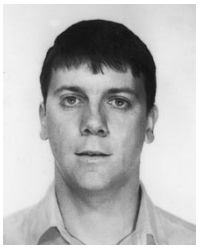

Marc Saillard received the Ph.D. degree in physics from the University of Aix-Marseille, France, in 1990.

From 1990 to 1997, he was a Researcher at the National Center for Scientific Research (CNRS) associated with the Laboratoire d'Optique Electromagnetique, Marseille, France. He is currently a Professor at the University of Provence in Marseille and is managing the Remote Sensing and Microwave Applications Team of the Fresnel Institute. His current research interests include inverse scattering, remote sensing, and wave propagation in random media and rough surfaces.

Dr. Saillard is a member of the Electromagnetic Academy.